ChemPubSoc Europe

DOI: 10.1002/chem.201602341

CHEMISTRY A European Journal Full Paper

Crystal Growth

Supramolecular Interactions Direct the Formation of Two Structural Polymorphs from One Building Unit in a One-Pot Synthesis

Ming-Yuan Zhang[+],[a] Zhenxing Wang[+],[c] Tao Yang[+],[a] Yuexing Zhang[+],[a] Xiong-Feng Ma,[a] Yi-Chen Sun,[c] Zhong-Wen Ouyang,[c] Mohamedally Kurmoo,[d] and Ming-Hua Zeng*[a, b]

Abstract: Two polymorphs of supramolecular isomers, a discrete *dimer* and a zig-zag *chain*, having the same chemical composition, $[Mn(Hbit)Cl_2]$ (Hbit = 1-methyl-2-(1*H*-1,2,3-triazol-4-yl)-1*H*-benzo[*d*]imidazole), were obtained solvothermally in a one-pot synthesis. The isomers differ in a number of ways: orange blocks versus pale-yellow needles, triclinic $P\bar{1}$ versus orthorhombic *Pbcn*, double μ_2-Cl versus alternate single and triple μ_2-Cl, coordination number 5 versus 6, and antiparallel versus parallel near-neighbor orientation of Hbit. The packing in each case is driven by the supramolecular interactions, H-bonds (N–H···Cl, C–H···Cl) and π···π overlaps, calculated to be in the range 20–36 kcal mol^{-1}. Calculations gave a difference of only 2 kcal mol^{-1} in favor of the *dimer*, which confirms with the observation of principally the *dimer* at short reaction time. ESI-MS spectra of the dissolved crystals reveal the same fragments with similar distributions. The presence of two fragments at *m/z* 286.96 $[Mn^{IV}(Hbit)Cl\text{-}2H]^+$ and 323.94 $[Mn^{III}(Hbit)Cl_2]^+$ indicates that $[Mn(Hbit)Cl_2]$ is the building unit in both cases; thus, the different orientations of the ligands lead to the two polymorphs stabilized by the respective supramolecular interactions. Importantly, the *chain* form represents the first example with alternate single and triple μ_2-Cl bridges. The magnetic interactions are weakly antiferromagnetic in both cases, with *J* in the range 0.07–0.34 cm^{-1}; however, high-field EPR analysis reveals moderate magneto-anisotropy with $D = 0.26(1)$ cm^{-1}, $E = 0.06(1)$ cm^{-1} and $D = 0.17(1)$ cm^{-1}, $E = 0.03(1)$ cm^{-1}, respectively.

Introduction

Crystal engineering studies in coordination chemistry have been undergoing an expansive development toward a promising future with designable structures of functional materials having desired physical and chemical properties.[1] The study of their self-assembly and control of crystallization processes is necessary and beneficial for the development of engineering crystals with predictable structures.[1c] Given the diversity and complexities of chemical reactions in solution and the uncertainties that exist with respect to the process of crystal formation, control over the final crystal structures remains a challenge.[2] It is even more so when different supramolecular isomers and polymorphs are formed in a one-pot reaction. Mechanistic study has some difficulties because of the intricate balance of moderate coordination bond versus the weak supramolecular interactions energies.

Among the studies of crystal engineering of coordination complexes, genuine supramolecular isomers based on identical chemical compositions but with structural difference provide an invaluable opportunity to study how a balance of energies between coordination bond, hydrogen bond, and π···π interactions can work in tandem in the self-assembly mechanism, crystal growth process and stabilities of the phases.[2b] Moreover, genuine supramolecular isomerism derived from a one-pot reaction of the reactants under certain conditions is such a system, and it can be used to study the self-assembly and crystal growth processes.

To understand the assembling process and the mechanism involved, there is a real need to overcome certain challenges with appropriate analytical methods and calculations.[3] In this respect, mass spectrometry[4] as well as theoretical studies[5] have been successful in previous works.

In this work, we report a unique system in which two supramolecular isomers were obtained from a one-pot synthesis. We

[a] M.-Y. Zhang,[+] Dr. T. Yang,[+] Dr. Y. Zhang,[+] X.-F. Ma, Prof. Dr. M.-H. Zeng
Key Laboratory for the Chemistry and Molecular Engineering of Medicinal Resources, Guangxi Normal University
Guilin, 541004 (P. R. China)

[b] Prof. Dr. M.-H. Zeng
College of Chemistry and Chemical Engineering
Hubei University, Wuhan, 430062 (P. R. China)
E-mail: zmh@mailbox.gxnu.edu.cn

[c] Dr. Z. Wang,[+] Y.-C. Sun, Prof. Dr. Z.-W. Ouyang
Wuhan National High Magnetic Field Center
Huazhong University of Science and Technology
Wuhan, 430074 (P. R. China)

[d] Dr. M. Kurmoo
Institut de Chimie de Strasbourg, CNRS-UMR 7177
Université de Strasbourg, 67070 Strasbourg (France)

[+] These authors contributed equally to this work.

Supporting information for this article is available on the WWW under http://dx.doi.org/10.1002/chem.201602341.

have studied their structural and magnetic properties and revealed the importance of different supramolecular interactions in directing the formation of the two polymorphs. The use of mass spectrometry analysis helped enable a process of formation to be proposed. The two polymorphs, orange block crystals (named *dimer*) and pale-yellow needles (named *chain*) of [Mn(Hbit)Cl_2], were obtained under solvothermal conditions (Scheme 1). The observation of such different shapes and colors for the two crystals encouraged us to study their crystal structures and formation processes. Single-crystal X-ray diffraction and structure analyses of the *dimer* and *chain* forms reveal that they are genuine supramolecular isomers without solvent or counter ion.

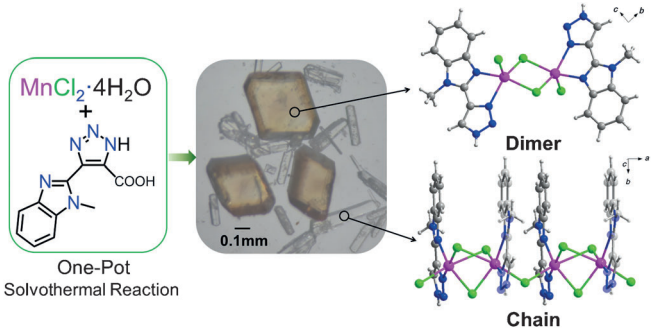

Scheme 1. Schematic presentation of the preparation of the *dimer* and *chain* by one-pot solvothermal reaction (left); local view of the mixture (middle); structure of the *dimer* and *chain* (right).

We highlight a strategy for investigating the bottom-up formation process of the supramolecular isomers using complementary techniques such as photography, ESI-MS, crystallography and theoretical calculations. To our knowledge, this is the first report concerning the process of formation of genuine supramolecular isomers using a bottom-up approach employing ESI-MS and theoretical calculations of the various bonding energies. Unusual alternative single and triple μ_2-Cl bridge were observed in the *chain* form. The magnetic properties of the *dimer* and *chain* are presented in addition to their high-field electron paramagnetic resonance (HF-EPR) spectra.

Results and Discussion

Crystal structures

X-ray structural analyses reveal that the *dimer* and *chain* crystallize in different space groups, $P\bar{1}$ and *Pbcn*, respectively. The asymmetric units of the *dimer* and *chain* consist of the same components, [Mn(Hbit)Cl_2]. In the structure of the *dimer*, the Mn^{2+} exhibits five-coordination (the degree of trigonality, $\tau = 0.45$)[6] with one terminal Cl, two μ_2-Cl and two N atoms from a chelating Hbit (Figure 1a). In the structure of the *chain*, Mn^{2+} displays six-coordination with four μ_2-Cl and two N atoms from a chelating Hbit (Figure 1b). In the *dimer*, the molecular unit can be considered as a combination of two [Mn(Hbit)Cl_2] fragments bridged by two μ_2-Cl, with orientations of two Hbit ligands being antiparallel (Figure 1c and e). Different from the *dimer*, the structure of the *chain* can be regarded as incorporating [Mn(Hbit)] units bridged by alternate triple and single μ_2-Cl in a one dimensional *chain*, with orientations of neighboring Hbit ligands being parallel (Figure 1d and f).

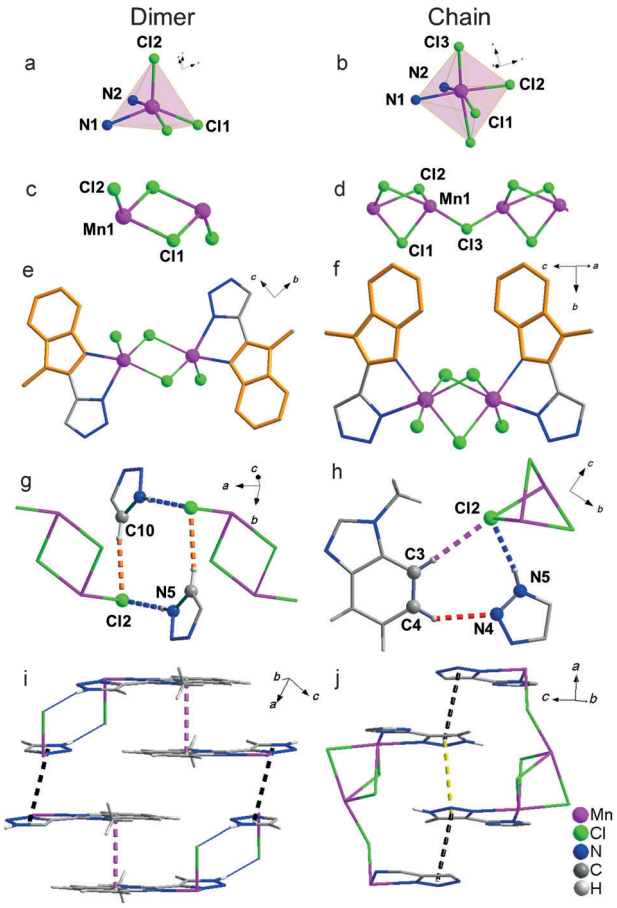

Figure 1. Structures of the *dimer* (left) and *chain* (right). a,b) Coordination mode of Mn^{2+}; c,d) connection mode of Cl^-; e,f) orientation mode of Hbit; g,h) hydrogen bond; i,j) π···π interaction.

In the structure of the *dimer*, there are two kinds of H-bond interactions within the molecular units (Figure 1g and Figure S1a in the Supporting Information). The intermolecular H-bonds, N–H···Cl (blue dotted line, $d_{N\cdots Cl} = 3.202(2)$ Å; ∡NHCl = 167.02(6)°), connect the neighbor units to form an infinite *chain*. The second H-bond originates from C–H···Cl (Figure 1g, orange dotted line) with C···Cl distance of 3.638(2) Å, and ∡CHCl = 168.44(7)°. Besides the H-bonds, there are two offset π···π stacking interactions in the structure (Figure 1i and Figure S1b). One is between two benzimidazole (bim) rings with a centroid-to-centroid distance of 3.743(2) Å (Figure 1i, pink dotted line), and an interplane distance of 3.483(2) Å. The second is between two triazole (C_2N_3) rings with a centroid-to-centroid distance of 3.690(3) Å (Figure 1i, black dotted line), and an interplane separation of 3.397(1) Å. These four intermolecular interactions are important factors for the crystallization process of the *dimer*. The C–H···π distance from the C(Me)

atom to the nearest aromatic ring is 4.514(2) Å, indicating there is no interaction. The four interactions in the structure of the *dimer* are shown in Figure S2.

In the *chain*, there are three kinds of H-bond to link the one-dimensional *chains* forming the 3D network structure (Figure 1 h and Figure S1c in the Supporting Information). The first is N–H···Cl (blue dotted line), in which N···Cl is 3.196(1) Å (∡CHN = 167.80(1)°). The second H-bond is C–H···N (Figure 1 h, red dotted line), with C···N distance of 3.328(1) Å, and ∡CHN = 146.02(2)°. The last H-bond stems from C–H···Cl (pink dotted line) with a C···Cl distance of 3.746(1) Å, and ∡CHCl = 176.39(1)°. There are two π···π stacking interactions in the structure of *chain* between pairs of triazole (C_2N_3) rings (Figure 1 j and Figure S1d). One has a centroid-to-centroid distance of 3.649(1) Å (Figure 1 j, black dotted line), and an interplane separation of 3.533(1) Å, and the second has 3.869(1) Å (Figure 1 i, yellow dotted line) and 3.255(1) Å, respectively. There is no π(bim)···π(bim) interaction in the structure of the *chain*. For C–H···π interactions (Figure S3, cyan and green dotted lines), the distances from C(Me) to the nearest benzene ring are 3.453(1) Å and 3.633(1) Å, indicating moderate interaction. The H-bonding and π···π interactions for the *dimer* and *chain* are listed in Table S1. It is noted that the H-bond and the interplane π···π interactions in the structures of *dimer* and *chain* are comparable to those reported previously.[7]

In the structure of the *dimer*, the Mn1···Mn1′ distance is 3.650(2) Å, and the Mn1-Cl1-Mn1′ angle is 93.83(2)°. In the *chain*, the Mn1···Mn1′ distance and Mn1-Cl-Mn1′ angles connected by triple μ_2-Cl are 3.340(1) Å and 77.99(2) and 82.76(2)° whereas those connected by single μ_2-Cl are 4.399(1) Å and 123.43(3)°. One of the Mn–Cl bond lengths of the triple μ_2-Cl bridge is 2.794(1) Å, which is longer than common coordination bonds, but still reasonable and comparable to those of reported compounds (Table S2 in the Supporting Information). In different kinds of μ_2-Cl bridge mode, the Mn1···Mn1′ distance and the Mn1-Cl-Mn1′ angles increase in the order, triple < double < single. This feature may relate to the stability of the three different kinds of μ_2-Cl bridge mode, and help us to understand the formation process. A survey of the literature from the CCDC database reveals there is only one ring that contains an alternative single and triple μ_2-Cl bridge (Figure S4).[8] It is notable that this is the first report of alternating single and triple μ_2-Cl bridging modes present in a one-dimensional *chain*. This new coordination mode for μ_2-Cl bridge is of interest for comparing the magnetic properties of the *dimer* and *chain* forms.

Moulton and Zaworotko have identified four types of supramolecular isomerism: structural, conformational, catenane, and optical, and noted that in-depth analyses of the crystal packing and intermolecular contacts are a prerequisite for a good understanding of supramolecular isomerism.[2a] These structural analyses have been performed in our case by considering: 1) the coordination mode of the metal ion, 2) the orientation mode of the ligand, 3) the connection mode of the anion, 4) the dimensionality, and 5) the space group. These aspects have been discussed to compare the two genuine supramolecular isomers. Of the papers with the key words 'supramolecular isomer', 60 report genuine structures (Table S3 in the Supporting Information) and 13 of them used a one-pot synthesis approach. The majority (39 of 60) are related to group IB and IIB elements and only two are Mn-based (Table S4 and Figure S5).[9] Table S5 lists the differences for the above criteria for compounds of these 13 reports. It is noted that *dimer* and *chain* forms possess the most differences compared with the other examples (Table S5). From a chemical synthesis point of view, the majority of papers relating to superamolecular isomerism focus on the crystallization process by controlling reaction conditions to isolate pure isomers.[10] However, few discussed or studied the mechanism of transformation process of the individual isomers in the context of the design and control of structures of coordination polymers.[2b,10]

Time-dependent photography

Time-dependent photography is a convenient way to monitor crystal growth and to help understand the crystallization process. A series of control experiments were therefore designed. The reactants (Hbitc, $MnCl_2{\cdot}4H_2O$) were stirred at room temperature in CH_3CN for 10 min prior to solvothermal treatment at 140 °C for different periods, 1, 4, 12, 24, and 72 h. Photographs of the solids and the mother liquors were taken (Figure S6 in the Supporting Information). As shown in Figure S6, Hbitc and $MnCl_2{\cdot}4H_2O$, are slightly dissolved in CH_3CN. After 12 h, the *dimer* is present but there is no *chain*, which appears by 24 h. For longer periods up to 72 h, the amount of *dimer* and *chain* as well as their crystal sizes increase. The constant presence of undissolved Hbitc and $MnCl_2{\cdot}4H_2O$ in the solvothermal process suggests that the slow decarboxylation process may be the limiting factor for the production of the two compounds.

Electrospray ionization mass spectrometry

For a better understanding of the formation process, solutions of the compounds were studied by ESI-MS. Selected crystals of the *dimer* and *chain* were dissolved in dimethyl sulfoxide (DMSO) and diluted with CH_3CN (Figure 2, and Figures S7–S9 and Table S6 in the Supporting Information). As shown in Figure 2, the spectra of *dimer* and *chain* forms suggest that they possess similar fragments. The peaks at *m/z* 200.09 and 245.93 correspond to $[(Hbit)+H]^+$ and $[Mn^{IV}Cl_3(CH_3OH)(H_2O)_3]^+$, respectively. They suggest that crystal formation proceeds following the decarboxylation of Hbitc to Hbit. The other peaks (*m/z* 215.02, 222.50, 286.96, and 323.94) were assigned to Mn-Hbit in which Mn^{II} was oxidized to either Mn^{III} or Mn^{IV} under ESI-MS conditions.[12] No peak was observed in the range *m/z* 500 to 700, which suggested that the *dimer* unit $[Mn_2(Hbit)_2Cl_4]$ is not present (Figure S7). From the decomposition behavior of the *dimer* and *chain*, with a top-down synthesis view, a hypothesis of the process of formation was therefore proposed. From the sparingly dissolved Hbitc and $MnCl_2{\cdot}4H_2O$ in CH_3CN, the former was decarboxylated to Hbit and coordinates to give the monomer $[Mn(Hbit)Cl_2]$ followed by dimerization or polymeri-

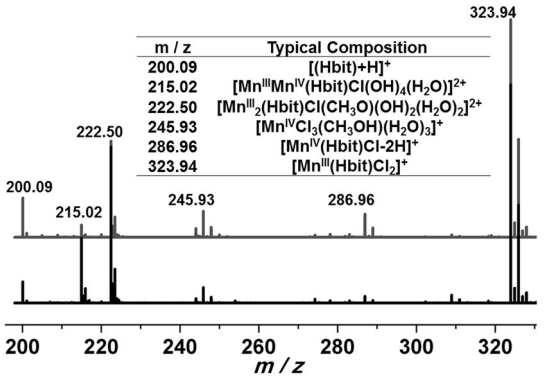

Figure 2. ESI-MS spectra of the solutions of dissolved crystals of the *dimer* (top) and *chain* (bottom) in DMSO and diluted in CH_3CN.

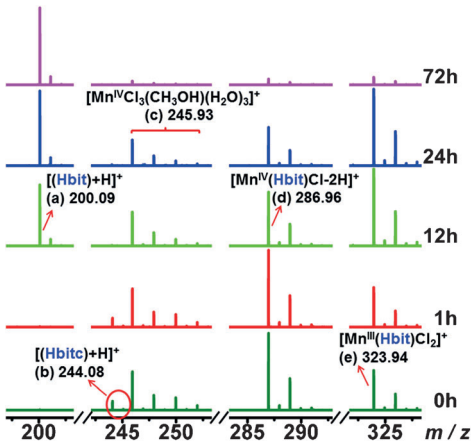

Figure 3. ESI-MS of the reaction solutions at different times.

zation depending on the orientation of the approaching monomer.

To support this hypothesis, an experiment was designed in which the reactants were stirred at room temperature prior to solvothermal treatment at 140 °C for different periods followed by filtration of the products from the mother liquors, and subsequent analysis by ESI-MS (Figure 3, and Figures S10, S11 and Table S7 in the Supporting Information). In the preparation of the mixture for solvothermal reaction (0 h), the peaks at *m/z* 244.08 (b) and 245.93 (c) corresponding to $[(Hbitc)+H]^+$ and $[Mn^{IV}Cl_3(CH_3OH)(H_2O)_3]^+$ indicates that Hbitc and $MnCl_2{\cdot}4H_2O$ partially dissolve in CH_3CN. Moreover, peaks at *m/z* 364.98 (f), 372.81 (g), 401.96 (h), 413.83 (i), and 448.82 (j), were all assigned to inorganic species, which confirms the dissolution of $MnCl_2{\cdot}4H_2O$ in CH_3CN under the reaction conditions (Figure S10). Those at *m/z* 286.96 (d) and 323.94 (e), corresponding to $[Mn^{IV}(Hbit)Cl\text{-}2H]^+$ and $[Mn^{III}(Hbit)Cl_2]^+$, indicate that Mn^{2+} ion is easy to coordinate to Hbit to form the building unit $[Mn(Hbit)Cl_2]$. It should be noted that, in the first 24 h, the Hbit related peaks (a, d, e) increase in intensity and Mn-related peaks (c, f, g, h, i, j) decrease in intensity, and the changes are correlated. This result indicates that dissolution of reactants and formation of products is essentially complete after 72 h. The reactant-related peaks are present, even after 24 h, when the *chain* appeared. This result suggests that $[Mn(Hbit)Cl_2]$ is the basic building unit for both the *dimer* and *chain* structures.

Two pivotal questions can be asked: Why can two markedly different compounds form under the same reaction conditions and why is crystallization of the *dimer* quicker than that of the *chain*? To address these two questions, complexation energies of the coordination bond, H-bond and π···π interaction in the structures were computed.

Theoretical calculations

The calculations based on optimized asymmetric units reveal that the *dimer* is about 2 kcal mol^{-1} (for each $Mn_2(Hbit)_2Cl_4$ *dimer*) more stable than the *chain*. This result corresponds well with the experimental finding that the *dimer* crystallizes out more easily and quickly than the *chain*. This is also in line with the previous conclusion that energy difference between supramolecular isomerism is generally very small, a matter of a few kcal mol^{-1}.[13]

Intermolecular interactions play an important role in the crystallization process. Computed complexation energies for interaction models within crystals of the *dimer* and *chain* are listed in Table 1 (Table S8 and Figure S12 in the Supporting Information). It is found that in the *dimer* crystal, Mn–Cl coordination bonds, π···π interaction between triazole rings, π···π interaction between benzimidazole rings, and N–H···Cl hydrogen bond have very similar complexation energies, lying in the range of 32–36 kcal mol^{-1}. The results also indicate that formation of the *dimer* is most likely the fusion of two $[Mn(Hbit)Cl_2]$ monomers, which are crystallized with the help of hydrogen-bonding and π···π interactions. This is in line with the MS results of solution of dissolved crystals in which the $[Mn(Hbit)Cl_2]$ fragment is the only prominent building unit (Figure 2 and Figure 3). However, as shown in Table 1, in the *chain* crystal, despite the fact that the complexation energy for forming triple μ_2-Cl bridges, with the value of 53 kcal mol^{-1}, is much larger than the interactions in *dimer*, the complexation energy for single μ_2-Cl bridge, N–H···Cl hydrogen bond, and triazole (C_2N_3) ring πM.>··π interaction, in the range of 20–30 kcal mol^{-1}, are much weaker in the *chain* than in the *dimer*. No π(bim)···π(bim) interaction is found in the *chain* crystal. When considering the difference between the monomer/segment of the *dimer* and *chain*, those of the two monomers in the *dimer* are the same with the two N and two Cl forming a tetrahedron configuration, whereas in the *chain* the two Mn–Cl bonds are rotated and one Mn–Cl bond is almost co-planar with the two N atoms. The deformation of $[Mn(Hbit)Cl_2]$ in the *chain* makes crystallization more difficult than in the *dimer*. Despite these differences between *dimer* and *chain*, it is expected that the formation of both crystals are the combined effect of Mn–Cl coordination bond and different weak interactions.

Hirshfeld surface analyses were also performed (Tables S9–S12 in the Supporting Information). Examination of decomposed 2D fingerprint plots shows that the dominant interaction in the packing of the *dimer* is Cl(inside Hirshfeld surface)···H(outside Hirshfeld surface) followed by H···H and H···Cl interactions, whereas the dominant interactions in the

Table 1. Calculated complexation energies of coordination-bond, hydrogen-bond and π···π interaction in the *dimer* and *chain*.

Structure	Bond	Energy[a]
Coordination bond		
dimer	Mn···$(\mu_2\text{-Cl})_D$···Mn	36[b]
chain	Mn···$(\mu_2\text{-Cl})_S$···Mn	30[c]
	Mn···$(\mu_2\text{-Cl})_T$···Mn	53[d]
Hydrogen bond		
dimer	N–H···Cl	33
	C–H···Cl	18
chain	N–H···Cl	20
	C–H···Cl	9
π···π interaction		
dimer	bim···bim	34
	C_2N_3···C_2N_3	32
chain	C_2N_3···C_2N_3	24
	C_2N_3···C_2N_3	22
	CH···Ph	15[e]

[a] Calculated complexation energy (kcal mol^{-1}). [b] Calculated complexation energy of double μ_2-Cl bridge. [c] Calculated complexation energy of single μ_2-Cl bridge. [d] Calculated complexation energy of triple μ_2-Cl bridge. [e] Calculated energy of two CH···Ph.

chain are H···H interactions followed by Cl···H. This corresponds well with the observation that Cl···H hydrogen bonds of the *dimer* have larger complexation energy than in the *chain*, whereas more π···π interactions are found in the *chain* than in the *dimer*.

Taken together, a plausible procedure is proposed for the process of formation of the *dimer* and *chain* (Figure S13 in the Supporting Information). There are two steps. The first step involves slow decarboxylation of Hbitc in the solution and formation of the $[Mn(Hbit)Cl_2]$ building unit. There are two possible ways to generate $[Mn(Hbit)Cl_2]$, first decarboxylation of Hbitc then coordination of Mn–N (Path A); inversely, coordination of Mn–N first then decarboxylation of Hbitc (Path B). The second step involved combination of $[Mn(Hbit)Cl_2]$ fragments. One possible way is that the $[Mn(Hbit)Cl_2]$ fragments quickly dimerize producing $Mn_2(Hbit)_2Cl_4$ in which the orientation of the Hbit ligand are antiparallel with recognition through intermolecular interactions. The other possible way is slow polymerization producing a triple μ_2-Cl bridge mode with Hbit oriented parallel while bridged by a single μ_2-Cl mode and packing through hydrogen-bonding and π···π interactions. A simple way of rationalizing the formation is to assume that the monomer adopts a tetrahedral coordination with two N and two Cl atoms. Given that the two N atoms form a chelate, only the Cl atoms can be moved to change the geometry. Thus, it is easier to distort the tetrahedron to a five-coordination to form the edge-sharing polyhedra of the *dimer* than it is to move the Cl to unfavorable positions to share faces of an octahedra in the *chain*. If the approach of the monomer to it neighbor has its Hbit ligand antiparallel (i.e., related by inversion symmetry) then the *dimer* is obtained because the polymerization is hampered by steric bulk. On the other hand if the approach is parallel (i.e., related by mirror symmetry) then the *chain* is favored because the free chlorine atoms are able to bond to more monomers leading to polymerization.

Magnetic properties

Magnetic susceptibilities for powdered samples of *dimer* and *chain* were measured in the temperature range of 2–300 K as shown in Figure 4. At 300 K, the *dimer* has a $\chi_m T$ value of 9.14 cm^3 mol^{-1} K, which is slightly higher than the spin-only value of 8.75 cm^3 mol^{-1} K for two noninteracting $S = 5/2$ Mn^{II} centers, whereas that of the *chain* at 300 K is 7.79 cm^3 mol^{-1} K, a value much lower than the spin-only value, indicating considerable antiferromagnetic interactions between neighboring Mn^{II} ions, which is further confirmed by the fast decreasing of $\chi_m T$ upon lowering temperature. The $\chi_m T$ value for the *dimer* is almost constant before exhibiting a rapid decrease around 20 K.

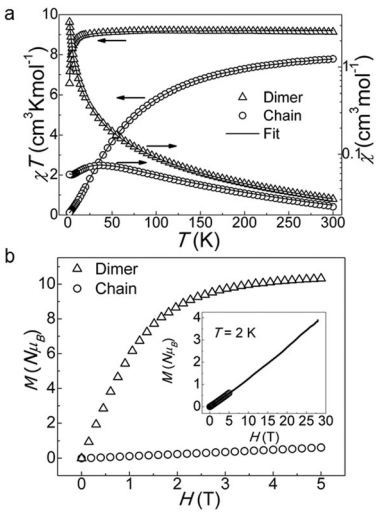

Figure 4. a) Temperature dependence of χ_m and $\chi_m T$ for the *dimer* (100 Oe) and the *chain* (1000 Oe). Solid lines represent the theoretical fits using the parameters listed in the text. b) Isothermal magnetizations for the *dimer* and *chain* at 2 K. Inset: pulsed-field magnetization curve for the *chain*.

Not considering single-ion zero-field splitting of Mn^{II}, the magnetic susceptibility data of the *dimer* and *chain* could be described by spin Hamiltonian (1) and (2) (see the Supporting Information), respectively, assuming all Mn^{II} ions have identical environments (see Figure 5 and Equation S1 in the Supporting Information). The best fit using the program PHI[14] resulted in $J = -0.07(1)$ cm^{-1} and $g = 2.05(2)$ for the *dimer* and $J_1' = -4.03(1)$ cm^{-1}, $J_2' = -0.34(1)$ cm^{-1}, and $g' = 2.05(2)$ for the *chain*. The very weak interaction for the *dimer* is consistent with the Goodenough–Kanamori rule[15] assuming a shift in angle associated with chlorine bridges compared to oxygen bridges. For the *chain*, if we only consider the Mn–Mn distance, the value of J_1' is quite consistent with the rule, but if we only consider the Mn-Cl-Mn angle, the large J_1' value is somehow debatable.

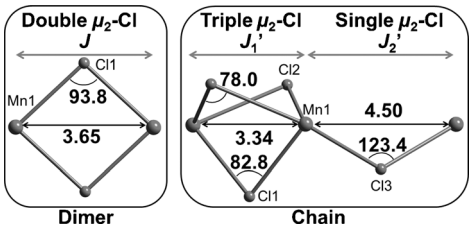

Figure 5. Definition of exchange couplings for the *dimer* and *chain* (distance, Å; angle, °).

Figure 4b shows the isothermal magnetization curves of the *dimer* and the *chain* measured at 2 K. The magnetization of the *dimer* reaches 10.33 μ_B at 5 T, consistent with the calculated value of 10.25 μ_B for Mn^{II} ($S=5/2$, $g=2.05$ derived from susceptibility measurements). In contrast, the magnetization of the *chain* increases almost linearly, and there is no hint of saturation even at 28 T (see inset of Figure 4b), which is in agreement with the large J as pointed out above. We note that the g and g'' values are larger than 2, which is probably due to the severe distortion of the local environments around Mn ions and their mixed coordination atoms (Figure 1a and b). The magneto-structural parameters of the reported compound containing the Mn-(μ_2-Cl)-Mn unit are listed in Table S13 in the Supporting Information.

The J, J_1', and J_2' values are comparable to those reported for Mn^{II} compounds (Table S13 in the Supporting Information); with a double μ_2-Cl bridge a change from ferromagnetic to antiferromagnetic behavior was observed, which was correlated with the Mn-Cl-Mn angle being less or more than 96° and Mn-Mn distance of ca. 3.7 Å. For a single μ_2-Cl bridge, there is no other compound similar to those reported here. There is only one of Mn-based compound with a triple μ_2-Cl bridge reported to date that has been magnetically characterized.[16] To our knowledge, the *chain* form is the first manganese magnetic material with alternate single and triple μ_2-Cl bridges in a *chain*.

High-field electron paramagnetic resonance

High-field electron paramagnetic resonance (HF-EPR) is a powerful method to characterize the Hamiltonian for molecular nanomagnets. To characterize the magneto-anisotropy parameters (D and E), originating from the unusual coordination geometries, the *dimer* and *chain* were subjected to HF-EPR (354 ± 1 GHz and 16 T (Figure 6). Both complexes exhibited very strong temperature dependence of EPR spectra in which the fine structure collapsed to a single resonance as the temperature was increased. This observation differs from those of the reported antiferromagnetically coupled {Mn_2} ($J=-3.35(10)$, $-15.5(5)$ cm^{-1})[17] and {Cr_2} ($J=-13.7(1)$ cm^{-1})[18] in which well-resolved EPR peaks are maintained up to 80 K. This difference is a direct consequence of the magnitude of exchange coupling that splits the levels, as illustrated in Figure S14.

For the *dimer*, two antiferromagnetically coupled Mn^{2+} ($S=5/2$) result in spin states of 0, 1, 2, 3, 4, 5, with $S=0$ as ground state at zero field and 0 K, whereas at high field $S=5$ becomes

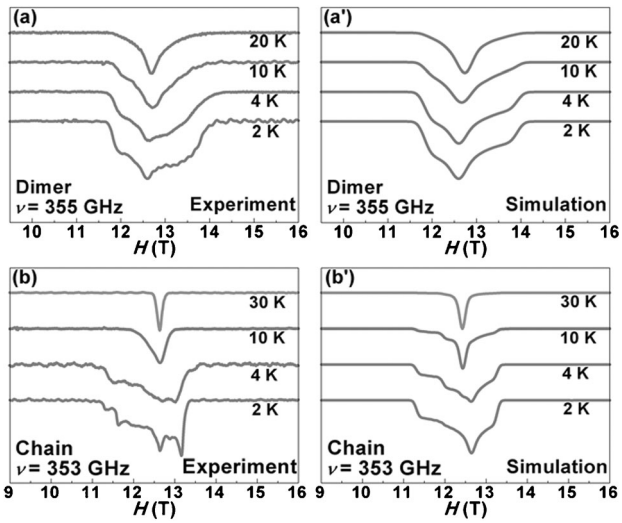

Figure 6. Experimental and simulated EPR spectra of the *dimer* (a, a') and *chain* (b, b').

the ground state with other spin states lying between the Zeeman levels of $m_S=\pm5$ for $S=5$. At the lowest temperature (2 K) used in EPR measurements (12.5 T/350 GHz), more than 99% of unpaired electrons are polarized on $m_S=-5$ level ($S=5$), so the EPR spectrum at 2 K is mainly from the $S=5$ state. As temperature increases, higher Zeeman levels are populated, and the EPR transitions from other spin states (i.e., $S=4$, 3…) will contribute to the overall EPR spectra. Considering the high degeneracy of excited spin states ($S=4$, 3, 2, 1) compared with that of the ground state ($S=5$), it is not surprising that EPR peaks collapse to center field if excited spin states have smaller zero-field splitting parameters. For the *chain*, the situation is more complicated because this 1D *chain* complex has two exchange coupling pathways. However, in the limit of $J_1' \gg J_2'$, the energy levels could still be understood as six groups for six spin states of 0, 1, 2, 3, 4, 5, similar to the *dimer*.

The EPR spectra of the *dimer* and *chain* could be described by using the spin Hamiltonian (3) and (4), respectively (see Equation S2). These two equations are expressed in terms of the spin operators of the individual ions. The S levels are not "pure" because the exchange couplings are not sufficiently large; therefore, the Zeeman levels cannot be handled by using the coupled-spin representation ("giant-spin" approximation), in which a separate spin Hamiltonian is used for each of the spin states. The exchange coupling constants (J, J_1', J_2') and g-values (g, g') obtained from magnetization measurements were used in the EPR simulations. As shown in Figure 6, EPR spectra of both the *dimer* and *chain* could be simulated for various temperatures. The slight mismatch of experimental and simulated spectra for the *chain* might be due to the overlook of exchange coupling between the next nearest neighbors. The resulting zero-field splitting parameters are: $D=0.26(1)$ cm^{-1}, $E=0.06(1)$ cm^{-1} for the *dimer*; $D'=0.17(1)$ cm^{-1}, $E'=0.03(1)$ cm^{-1} for the *chain*. The magnitudes of these values are close to the reported values for Mn *dimers* ($D=0.312$ cm^{-1}, $E=0.005$ cm^{-1}).[16b] We also tried to use the obtained D and E

values to refine the fitting of susceptibility data, and found that the addition of *D* and *E* values to the fitting processes does not significantly change the fitting results as expected. HF-EPR studies not only proved that the model used in the analysis of magnetization is valid, but also provided important information of the single ion anisotropies. Further studies of the correlations between crystal field and magnetic anisotropy need theoretical calculations, which is beyond the scope of the current work.

Conclusions

Two polymorphs, obtained from the same reagents in a one-pot synthesis, consist of the same chemical compositions and can be described as genuine supramolecular isomers, have been characterized. A combination of complementary techniques and calculations revealed how the subtle balance of energies of the different bonding interactions, dative and supramolecular, can direct the different arrangements. Whereas mass spectrometry identified the building unit to be the same, a complete study of the structure backed by estimation of the energies reveals the way the two polymorphs are generated. Thus, the results provide evidence for the formation of the polymorphs through decarboxylation of ligand, complexation to the monomer, and its combination to *dimer* and *chain* by the two energetically similar fusion steps. The control of the balance in energies may be a strategy that can be extended to investigate the design of multifunctional materials through crystal structure prediction and crystal engineering.

Experimental Section

Materials and measurements

All the reagents were obtained from commercial sources and used without further purification. Hbitc was synthesized according a reported procedure (see the Supporting Information). Elemental analyses were carried out with a Vario EL Cube. Thermogravimetric analysis (TGA) was performed in a flow of nitrogen at a heating rate of 5 °C min^{-1} with a NETZSCH TG 209 F3. Infrared spectra were collected by transmission through KBr pellets with a PE Spectrum FTIR spectrometer (400–4000 cm^{-1}). The X-ray powder diffraction (PXRD) patterns were recorded at 293 K with a Rigaku D/max-IIIA diffractometer ($Cu_{K\alpha}$, $\lambda = 1.54056$ Å). Magnetization of polycrystalline samples was measured in the temperature range of 2.0–300 K and field range ± 50 kOe with a Quantum Design MPMS XL-5 SQUID magnetometer. Magnetization and electron paramagnetic resonance (HF-EPR) were measured with locally developed instruments with pulsed-magnetic fields up to 30 Tesla.[19]

Syntheses of *dimer* and *chain*

$MnCl_2{\cdot}4H_2O$ (99 mg, 0.5 mM), Hbitc (65 mg, 0.25 mM), and acetonitrile (18 mL) were stirred for 10 min, then transferred in a 25 mL Teflon-lined stainless steel reactor and sealed, followed by heating at 140 °C for 3 days, then cooled to RT. Both orange block (*dimer*) and pale-yellow needles (*chain*) crystals were obtained, which were separated manually under an optical microscope. The Hbit ligand was generated in situ from Hbitc by decarboxylation under solvothermal conditions (Figure S15 in the Supporting Information). Phase purity of the *dimer* and *chain* were checked by PXRD (Figures S16 and S17). The yield varied slightly for each batch even under similar conditions. There was no solvent in the structures of either *dimer* or *chain*, which was confirmed by thermogravimetric analyses (TGA, Figures S18 and S19) and by elemental analyses (EA).

Dimer $Mn_2(Hbit)_2(\mu_2\text{-}Cl)_2Cl_2$: Yield: 51.2 mg (63% based on Hbitc); elemental analyses calcd. (%) for $Mn_2C_{20}H_{18}N_{10}Cl_4$ C, 36.95; H, 2.79; N, 21.55; found: C, 36.72; H, 2.91; N, 21.44. IR (KBr): 3092 (s), 2923 (s), 1509 (m), 1462 (m), 801 (m), 750 (m) cm^{-1}.

Chain $[Mn_2(Hbit)_2(\mu_2\text{-}Cl)_4]_n$: Yield: 5.4 mg (6.6% based on Hbitc); elemental analyses calcd. (%) for $Mn_2C_{20}H_{18}N_{10}Cl_4$: C, 36.95; H, 2.79; N, 21.55; found: C, 36.69; H, 3.01; N, 22.02; IR (KBr): 3099 (s), 2924 (s), 1516 (m), 1465 (m), 820 (m), 763 (m) cm^{-1}.

Crystallographic studies

Single-crystal X-ray diffraction data for *dimer* and *chain* were collected with a Bruker Smart Apex CCD and an Agilent Supernova CCD diffractometer, respectively. Both employed graphite-monochromated $Mo_{K\alpha}$ radiation. The structures were solved by direct methods and refined by least-squares. The $F_o - F_c$ maps identified all the hydrogen atoms with electron densities higher than 2σ level. In the structure of the *chain*, Cl1 and Cl3 atoms located at special positions; their site occupation factors were 0.5. Selected bond lengths and angles for the *dimer* and *chain* are listed in Table S14 in the Supporting Information. The supplementary crystallographic data can be found in the Supporting Information. CCDC 1472804 (*dimer*) and 1472803 (*chain*) contain the supplementary crystallographic data for this paper. These data are provided free of charge by The Cambridge Crystallographic Data Centre.

Crystal data for $C_{20}H_{18}Cl_4Mn_2N_{10}$ (*dimer*) (650.12 g mol^{-1}): triclinic; space group $P\bar{1}$ (no. 2); $a = 7.535(6)$ Å, $b = 8.556(7)$ Å, $c = 10.541(9)$ Å, $\alpha = 81.462(1)^\circ$, $\beta = 74.65(1)^\circ$, $\gamma = 73.24^\circ$; $V = 625.6(9)$ Å^3; $Z = 1$; $T = 296(2)$ K; $\mu(Mo_{K\alpha}) = 1.469$ mm^{-1}; $D_{calcd} = 1.726$ g cm^{-3}; 7010 reflections measured ($4.020^\circ \le 2\Theta \le 52.692^\circ$), 2522 ($R_{int} = 0.017$) which were used in all calculations. The final R_1 was 0.0223($I > 2\sigma(I)$) and wR_2 was 0.0667(all data).

Crystal data for $C_{20}H_{18}Cl_4Mn_2N_{10}$ (*chain*) (650.12 g mol^{-1}): orthorhombic; space group *Pbcn* (no. 60); $a = 6.9594(2)$ Å, $b = 21.3694(6)$ Å, $c = 16.2348(5)$ Å; $V = 2414.4(1)$ Å^3; $Z = 4$; $T = 293(2)$ K; $\mu(Mo_{K\alpha}) = 1.522$ mm^{-1}; $D_{calcd} = 1.789$ g cm^{-3}; 25 177 reflections measured ($6.650^\circ \le 2\Theta \le 57.778^\circ$), 3061 ($R_{int} = 0.036$) which were used in all calculations. The final R_1 was 0.0297($I > 2\sigma(I)$) and wR_2 was 0.0714(all data).

Computational methodology

The geometries of both *dimer* and *chain* unit cell were optimized by using generalized gradient approximation functionals-BE with Grimme's G06 dispersion correction and effective core potential for Mn, and DNP basis set for other elements. Complexation energies between $[Mn(Hbit)Cl_2]$ segments in the *dimer* and *chain* and their possible direct-contact neighbors (with shortest distance less than 5 Å) were calculated by using the B3LYP functional adding the D3 version of Grimme's dispersion with Becke–Johnson damping and SDD ECP for Mn and 6–311G(d) basis sets for other elements using Gaussian 09 software.[20] These results make it possible to separate each interaction among the complex set of interaction energies within the crystal structures. In all the calculations, high spin of 5/2 was used for the system containing one Mn atom, whereas spin-polarized singlet (neighbor Mn atoms have spin of 5/2 and −5/2) and a total spin of 0 was used for systems with more than one Mn

atom. Basis set superposition error (BSSE) was corrected by counterpoise method, in which both Mn atoms have high spin of 5/2. The superposition error is very small and negligible, as a result, only the complexation energy without BSSE are used during the discussion. Hirshfeld surface analysis is performed by using CrystalExplorer.[21]

Acknowledgements

This work was supported by the National Science Foundation for Distinguished Young Scholars of China (No. 21525101), the NSF of China and Guangxi Province (No. 91122032, 2014GXNSFFA118003), the BAGUI scholar program (2014A001) and the Project of Talents Highland of Guangxi Province. This work is also supported by Opening Project of Wuhan National High Magnetic Field Center (Grant No. 2015KF05), and Huazhong University of Science and Technology. We thank Professor Hiroyuki Nojiri (Tohoku University) for the high-field magnetization measurements. We also acknowledge the group of Professor Jianzhuang Jiang (University of Science and Technology Beijing; USTB) for providing computational resources and thank Dr. Dongdong Qi for stimulating discussions. M.K. is supported by CNRS-France. The authors declare no competing financial interest.

Keywords: crystal engineering · crystal growth · isomers · magnetic properties · supramolecular interactions

[1] a) S. R. Batten, S. M. Neville, D. R. Turner, *Coordination Polymers: Design, Analysis and Application*, RSC, Cambridge, **2008**; b) J. Bernstein, R. J. Davey, J. O. Henck, *Angew. Chem. Int. Ed.* **1999**, *38*, 3440 – 3461; *Angew. Chem.* **1999**, *111*, 3646 – 3669; c) G. R. Desiraju, *Angew. Chem. Int. Ed.* **2007**, *46*, 8342 – 8356; *Angew. Chem.* **2007**, *119*, 8492 – 8508; d) G. R. Desiraju, *J. Am. Chem. Soc.* **2013**, *135*, 9952 – 9967.

[2] a) B. Moulton, M. J. Zaworotko, *Chem. Rev.* **2001**, *101*, 1629 – 1658; b) J.-P. Zhang, X.-C. Huang, X.-M. Chen, *Chem. Soc. Rev.* **2009**, *38*, 2385 – 2396.

[3] H. N. Miras, E. F. Wilson, L. Cronin, *Chem. Commun.* **2009**, *11*, 1297 – 1311.

[4] a) Y.-L. Zhou, M.-H. Zeng, L.-Q. Wei, B.-W. Li, M. Kurmoo, *Chem. Mater.* **2010**, *22*, 4295 – 4303; b) L.-Q. Wei, K. Zhang, Y.-C. Feng, Y.-H. Wang, M.-H. Zeng, M. Kurmoo, *Inorg. Chem.* **2011**, *50*, 7274 – 7283; c) L.-Q. Wei, B.-W. Li, S. Hu, M.-H. Zeng, *CrystEngComm* **2011**, *13*, 510 – 516; d) Y.-Q. Hu, M.-H. Zeng, K. Zhang, S. Hu, F.-F. Zhou, M. Kurmoo, *J. Am. Chem. Soc.* **2013**, *135*, 7901 – 7908; e) K. Zhang, M. Kurmoo, L.-Q. Wei, M.-H. Zeng, *Sci. Rep.* **2013**, *3*, 3516.

[5] a) Y. Zhang, X. Cai, P. Yao, H. Xu, Y. Z. Bian, J. Z. Jiang, *Chem. Eur. J.* **2007**, *13*, 9503 – 9514; b) Y. Zhang, B. Champagne, *J. Phys. Chem. C* **2013**, *117*, 1833 – 1848.

[6] A. W. Addison, T. N. Rao, J. Reedijk, J. van Rijn, G. C. Verschoor, *J. Chem. Soc. Dalton Trans.* **1984**, 1349 – 1356.

[7] a) C. Janiak, *J. Chem. Soc. Dalton Trans.* **2000**, 3885 – 3896; b) G. A. Jeffrey, *Crystallogr. Rev.* **2003**, *9*, 135 – 176.

[8] J. T. Golden, D. N. Kazul'kin, B. L. Scott, A. Z. Voskoboynkov, C. J. Burns, *Organometallics* **2003**, *22*, 3971 – 3973.

[9] S.-C. Manna, E. Zangrando, J. Ribas, N.-R. Chaudhuri, *Eur. J. Inorg. Chem.* **2008**, 1400 – 1405.

[10] a) S. Masaoka, D. Tanaka, Y. Nakanishi, S. Kitagawa, *Angew. Chem. Int. Ed.* **2004**, *43*, 2530 – 2534; *Angew. Chem.* **2004**, *116*, 2584 – 2588; b) D.-F. Sun, Y.-X. Ke, T. M. Mattox, B. A. Ooro, H.-C. Zhou, *Chem. Commun.* **2005**, 5447 – 5449; c) Z.-M. Hao, X.-M. Zhang, *Cryst. Growth Des.* **2007**, *7*, 64 – 68; d) S. Wang, H.-Y. Zang, C.-Y. Sun, G.- J. Xu, X.-L. Wang, K.-Z. Shao, Y.-Q. Lan, Z.-M. Su, *CrystEngComm* **2010**, *12*, 3458 – 3462; e) D.-L. Deng, L.-L. Liu, B.-M. Ji, G.-J. Yin, C.-X. Du, *Cryst. Growth Des.* **2012**, *12*, 5338 – 5348; f) L.-L. Han, T.-P. Hu, K. Mei, Z.-M. Guo, C. Yin, Y.-X. Wang, J. Zheng, X.-P. Wang, D. Sun, *Dalton Trans.* **2015**, *44*, 6052 – 6061.

[11] a) L. Cheng, W.-X. Zhang, B.-H. Ye, J.-B. Lin, X.-M. Chen, *Inorg. Chem.* **2007**, *46*, 1135 – 1143; b) J.-P. Zhang, X.- L. Qi, C.-T. He, Y. Wang, X.-M. Chen, *Chem. Commun.* **2011**, *47*, 4156 – 4158.

[12] a) C. Ritchie, E. M. Burkholder, D.-L. Long, D. Adam, P. Kögerler, L. Cronin, *Chem. Commun.* **2007**, 468 – 470; b) Y.-K. Deng, H.-F. Su, J.-H. Xu, W.-G. Wang, M. Kurmoo, S.-C. Lin, Y.-Z. Tan, J. Jia, D. Sun, L.-S. Zheng, *J. Am. Chem. Soc.* **2016**, *138*, 1328 – 1334.

[13] a) J. Bernstein, J. D. Dunitz, *Acc. Chem. Res.* **1995**, *28*, 193 – 200; b) A. Nangia, *Acc. Chem. Res.* **2008**, *41*, 595 – 604.

[14] N. F. Chilton, R. P. Anderson, L. D. Turner, A. Soncini, K. S. Murray, *J. Comput. Chem.* **2013**, *34*, 1164 – 1175.

[15] a) J. B. Goodenough, *Magnetism and the Chemical Bond*, Wiley, New York, **1963**; b) J. Kanamori, *J. Phys. Chem. Solids* **1959**, *10*, 87 – 98; c) J. Kanamori, in *Magnetism* (Eds.: G. T. Rado, H. Suhl), *Vol. I*, Academic Press, New York, **1963**, Ch. 4, p. 127.

[16] U. Bossek, D. Nühlen, E. Bill, T. Glaser, C. Krebs, T. Weyhermüller, K. Wieghardt, M. Lengen, A. X. Trautwein, *Inorg. Chem.* **1997**, *36*, 2834 – 2843.

[17] a) V. G. Makhankova, A. O. Beznischenko, V. N. Kokozay, R. I. Zubatyuk, O. V. Shishkin, J. Jezierska, A. Ozarowski, *Inorg. Chem.* **2008**, *47*, 4554 – 4563; b) D. L. Reger, A. E. Pascui, M. D. Smith, J. Jezierska, A. Ozarowski, *Inorg. Chem.* **2012**, *51*, 11820 – 11836.

[18] V. V. Semenaka, O. V. Nesterova, V. N. Kokozay, V. V. Dyakonenko, R. I. Zubatyuk, O. V. Shishkin, R. Boča, J. Jezierska, A. Ozarowski, *Inorg. Chem.* **2010**, *49*, 5460 – 5471.

[19] a) H. Nojiri, K.-Y. Choi, N. Kitamura, *J. Magn. Magn. Mater.* **2007**, *310*, 1468 – 1472; b) H. Nojiri, Z.-W. Ouyang, *Thz. Sci. Techn.* **2012**, *5*, 1 – 10.

[20] Gaussian 09, Revision D.01, M. J. Frisch, G. W. Trucks, H. B. Schlegel, G. E. Scuseria, M. A. Robb, J. R. Cheeseman, G. Scalmani, V. Barone, B. Mennucci, G. A. Petersson, H. Nakatsuji, M. Caricato, X. Li, H. P. Hratchian, A. F. Izmaylov, J. Bloino, G. Zheng, J. L. Sonnenberg, M. Hada, M. Ehara, K. Toyota, R. Fukuda, J. Hasegawa, M. Ishida, T. Nakajima, Y. Honda, O. Kitao, H. Nakai, T. Vreven, J. A. Montgomery, Jr., J. E. Peralta, F. Ogliaro, M. Bearpark, J. J. Heyd, E. Brothers, K. N. Kudin, V. N. Staroverov, R. Kobayashi, J. Normand, K. Raghavachari, A. Rendell, J. C. Burant, S. S. Iyengar, J. Tomasi, M. Cossi, N. Rega, J. M. Millam, M. Klene, J. E. Knox, J. B. Cross, V. Bakken, C. Adamo, J. Jaramillo, R. Gomperts, R. E. Stratmann, O. Yazyev, A. J. Austin, R. Cammi, C. Pomelli, J. W. Ochterski, R. L. Martin, K. Morokuma, V. G. Zakrzewski, G. A. Voth, P. Salvador, J. J. Dannenberg, S. Dapprich, A. D. Daniels, Ö. Farkas, J. B. Foresman, J. V. Ortiz, J. Cioslowski, D. J. Fox, Gaussian, Inc., Wallingford CT, 2009.

[21] CrystalExplorer (Version 3.1), S. K. Wolff, D. J. Grimwood, J. J. McKinnon, M. J. Turner, D. Jayatilaka, M. A. Spackman, University of Western Australia, **2012**.

Received: May 17, 2016
Published online on ■■ ■■, 0000

FULL PAPER

Crystal clear: Two genuine supramolecular isomers, *dimer* and *chain*, possessing identical chemical components, $[Mn(Hbit)(Cl)_2]$, form from the same building unit. Formation of the structures are driven by competition of energetically similar coordination bonds with the H-bond and π···π supramolecular interactions, leading to different coordination numbers and distortions of Mn^{2+} centers, orientation modes of chelating Hbit and different distributions of μ_2-Cl bridges.

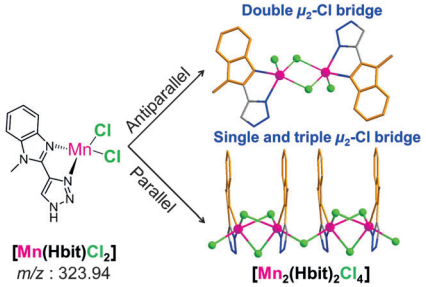

Crystal Growth

*M.-Y. Zhang, Z. Wang, T. Yang, Y. Zhang, X.-F. Ma, Y.-C. Sun, Z.-W. Ouyang, M. Kurmoo, M.-H. Zeng**

■■ – ■■

Supramolecular Interactions Direct the Formation of Two Structural Polymorphs from One Building Unit in a One-Pot Synthesis